J. Fluid Mech. (2001), *vol.* 438, *pp.* 213–230. Printed in the United Kingdom

Downstream and upstream influence in river meandering. Part 2. Planimetric development

By G. SEMINARA[1], G. ZOLEZZI[1]†, M. TUBINO[2] AND D. ZARDI[2]

[1]Dipartimento di Ingegneria Ambientale, Università di Genova, Via Montallegro 1, 16122, Genoa, Italy

[2]Dipartimento di Ingegneria Civile e Ambientale, Università di Trento, Via Mesiano 77, 38050, Trento, Italy

(Received 20 July 1999 and in revised form 10 December 2000)

The exact solution of the problem of river morphodynamics derived in Part 1 is employed to formulate and solve the problem of planimetric evolution of river meanders. A nonlinear integrodifferential evolution equation in intrinsic coordinates is derived. An exact periodic solution of such an equation is then obtained in terms of a modified Fourier series expansion such that the wavenumbers of the various Fourier modes are time dependent. The amplitudes of the Fourier modes and their wavenumbers satisfy a nonlinear system of coupled ordinary differential equations of the Landau type. Solutions of this system display the occurrence of two possible scenarios. In the sub-resonant regime, i.e. when the aspect ratio of the channel is smaller than the resonant value, meandering evolves according to the classical picture: a periodic train of small-amplitude sine-generated meanders migrating downstream evolve into the classical, upstream skewed, train of meanders of Kinoshita type. Evolution displays all the experimentally observed features: the meander growth rate increases up to a maximum and then decreases, while the migration speed decreases monotonically. No equilibrium solutions are found. In the super-resonant regime the picture is essentially reversed: downstream skewing develops while meanders migrate upstream.

Numerical solutions of the planimetric evolution equation are obtained for the case when the initial channel pattern exhibits random small perturbations of the straight configuration. Under these conditions, the evolution displays the typical features of solutions of the Ginzburg–Landau equation, in particular, the occurrence of spatial modulations of the meandering pattern which organizes itself in the form of wavegroups. Furthermore, multiple loops develop in the advanced stage of meander growth.

1. Introduction

The shape of river meanders is the result of a self-forming process essentially consisting of an intermittent sequence of erosion of concave banks and accretion associated with deposition at convex banks. In the absence of significant geological constraints or anthropization, meanders develop typically regular forms, though examples have been reported of rivers for which spectral analysis has not revealed the

† Present address: Dipartimento di Ingegneria Civile e Ambientale, Università di Trento, Via Mesiano 77, 38050, Trento, Italy.

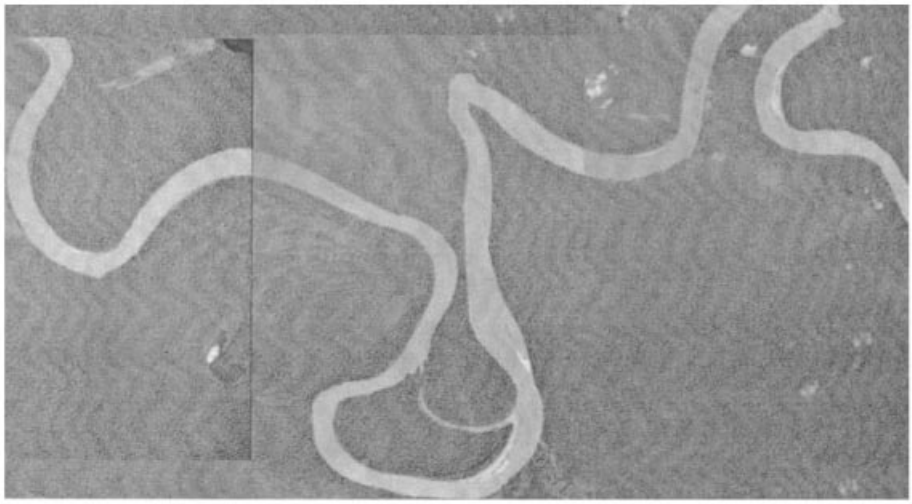

FIGURE 1. An example of a super-resonant downstream skewed meander loop. Raggi Island reach, Fly River, Papua New Guinea. Flow is from right to left. (Courtesy of W. Dietrich.)

existence of any dominant spatial scale (Speight 1965, 1967). Langbein & Leopold (1964) suggested, on the basis of field observations, that the channel axis of meandering rivers can often be mathematically described by what they called a 'sine-generated curve', a line characterized by curvature which varies sinusoidally as a function of arclength. Meanders are typically skewed upstream, a feature which allows us to detect flow direction from an aerial view. The observations of Kinoshita (1961) suggest that the inclusion of third harmonics correcting the sine-generated curve accounts for the above skewing and for the pronounced fattening exhibited by real meanders. Hence, Kinoshita (1961) writes

$$\mathscr{C}^* = \mathscr{C}_0^* \left[\cos(\lambda^* s^*) - \mathscr{C}_F \cos(3\lambda^* s^*) - \mathscr{C}_S \sin(3\lambda^* s^*)\right], \tag{1.1}$$

where $\mathscr{C}^*$ is curvature, λ^* is the intrinsic meander wavenumber, s^* is arclength, $\mathscr{C}_F$ and $\mathscr{C}_S$ are called 'fattening' and 'skewing' coefficients, respectively, and an asterisk denotes dimensional quantities.

A second important field observation which applies to freely developing meanders is the reduction of the downstream migration rate (Kinoshita 1961) and the initial increase and eventual decay of lateral migration rate (Nanson & Hickin 1983).

Though the latter observations depict the more common typology of planimetric development of river meanders, it is not uncommon to observe the opposite behaviour. Figure 1 shows an example of one downstream skewed meander loop in the so-called Raggi Island reach (Fly River, Papua New Guinea) (courtesy of W. Dietrich); moreover, 'multiple loops' are also often observed in nature (see figure 2). This was previously pointed out by Brice (1974), who discussed the typical shape of meander loops and showed (his figure 1) examples of downstream skewed meander loops and of multiple loops.

The above simple field observations pose various questions. Are the sine-generated curve and Kinoshita curve pure empirical correlations? Why are even harmonics absent, and harmonics higher than the third apparently negligible? What determines the type of meander development? Why are most meanders upstream skewed while others are skewed downstream? Is the migration speed invariably positive? Can we

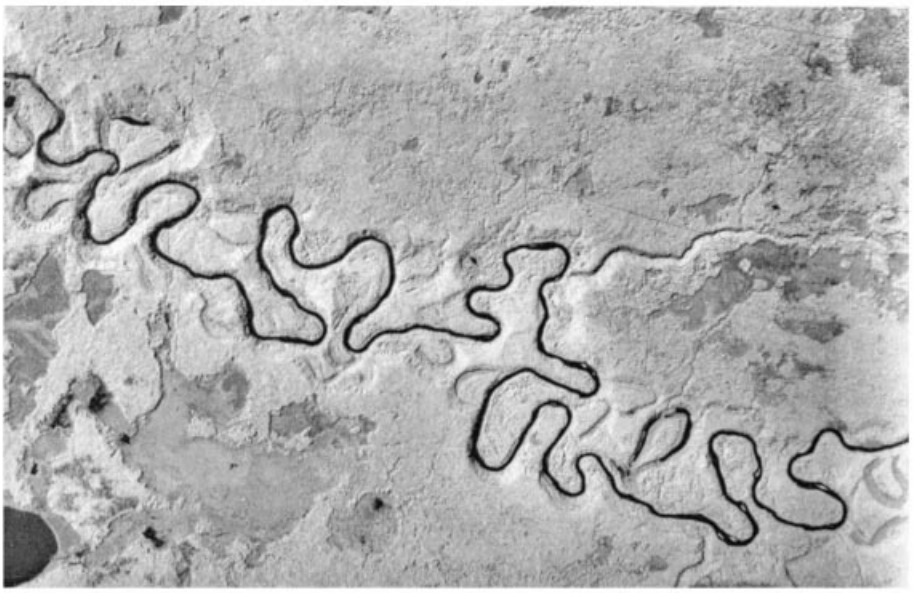

FIGURE 2. Reach of the meandering Notikewin River (Canada): multiple loops occur. Flow is from right to left. (Courtesy of G. Parker.)

predict the development of the above shapes and the time variation of lateral and longitudinal migrations on the basis of a mechanistic model?

Some of the above questions have already been posed and answered in a series of important papers published by Parker and his coworkers in the 1980s (Ikeda, Parker & Sawai 1981; Parker, Sawai & Ikeda 1982; Parker, Diplas & Akiyama 1983; Parker & Andrews 1986).

We wish to revisit the above problems in the light of recent developments of the theory of river meandering (see Part 1, Zolezzi & Seminara 2001), which will now be set as the basis of a nonlinear theory of bend instability able to cover both sub-resonant and super-resonant conditions. Our final aim is to construct a mechanistic model of river development able to answer the questions posed above. It will appear that in the sub-resonant case, our nonlinear solution does indeed predict the development of meander shapes of the Kinoshita type from incipient formation to cutoff. The downstream migration rate is invariably found to decline while the transverse migration rate increases to a maximum and eventually decays. The latter findings are in complete agreement with observations.

In the super-resonant case, meanders are found to develop a shape which is downstream skewed and migrates upstream. However, as meanders develop, the associated reduction of the average channel slope leads to increasing values of the flow depth, hence, to decreasing values of the width to depth ratio. As a result, super-resonant meanders tend to cross the resonant barrier and recover a sub-resonant behaviour in later stages of meander growth. The occurrence of multiple loops is also predicted.

The rest of the paper proceeds as follows. In § 2, we derive a new intrinsic formulation of the planimetric evolution equation which is given an exact analytic periodic solution in § 3. Results are described in § 4 and in § 5 for meander trains starting from periodic and random initial configurations, respectively, both in the sub-resonant and

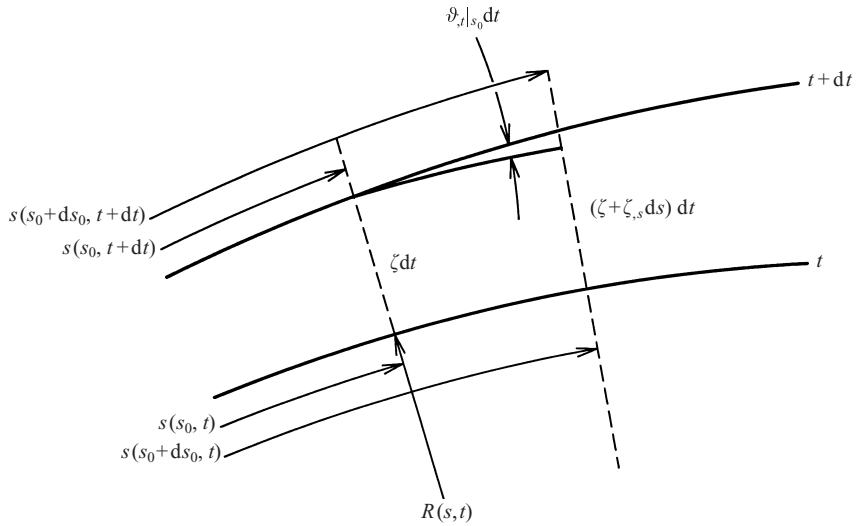

FIGURE 3. Notation of planimetric evolution of channel axis.

in the super-resonant cases. Finally in § 6, a discussion of the various aspects which still warrant attention along with some conclusions complete the paper.

2. An intrinsic formulation of the planimetric evolution equation of meandering channels

A Cartesian form of the planimetric evolution equation of meandering channels was first derived by Ikeda *et al.* (1981). Here we present an intrinsic formulation which turns out to take a relatively simple form and appears to be the most suitable one to explain the field observations of Langbein & Leopold (1964) and Kinoshita (1961).

Let ζ denote the lateral migration rate of the channel scaled by some typical speed U_0^*, say the average uniform speed of the flow in the initially straight channel. Furthermore, let s be the curvilinear coordinate which identifies the location at time t of the cross-section which was located at s_0 initially, the quantities s and t being made dimensionless by B^* and (B^*/U_0^*), respectively, with B^* the half-channel width. The quantity ζ will be a function of s and t through its dependence on the distribution of bank erosion, hence on the characteristics of the flow field, of bed topography and of the geological texture of the banks.

Figure 3 suggests that the relative transverse displacement of two neighbouring points of the channel axis, say s and $s+\mathrm{d}s$, in the infinitesimal time interval $\mathrm{d}t$ is related to the infinitesimal variation of the angle ϑ which the tangent to the channel axis forms with some Cartesian axis x, in the form

$$\zeta_{,s}\mathrm{d}s\mathrm{d}t = (\vartheta_{,t}|_{s_0}\mathrm{d}t)\mathrm{d}s, \tag{2.1}$$

where $\vartheta_{,t}|_{s_0}$ is a Lagrangian derivative. Transforming the latter equation into Eulerian form we find from (2.1)

$$\vartheta_{,t} + \vartheta_{,s}\frac{\mathrm{d}s}{\mathrm{d}t} = \zeta_{,s}. \tag{2.2}$$

The material derivative of the arclength $\mathrm{d}s/\mathrm{d}t$ is then readily obtained noting that in the interval $\mathrm{d}t$ each infinitesimal portion of the channel axis increases its initial

length ds by an amount d(ds) which reads

$$\mathrm{d}(\mathrm{d}s) = \frac{(\zeta \mathrm{d}t)}{R}\mathrm{d}s = -\zeta \vartheta_{,s}\, \mathrm{d}s\mathrm{d}t, \tag{2.3}$$

with R the dimensionless local radius of curvature, scaled by B^*.

Hence,

$$\frac{\mathrm{d}s}{\mathrm{d}t} = -\int_0^s \zeta \vartheta_{,s}\mathrm{d}s \tag{2.4}$$

and (2.2) becomes

$$\vartheta_{,t} - \vartheta_{,s}\int_0^s \zeta \vartheta_{,s}\mathrm{d}s = \zeta_{,s}. \tag{2.5}$$

Equation (2.5) is the intrinsic form of the planimetric evolution equation of meandering channels. It may be useful to point out that the latter equation applies at any stage of meander evolution (preceding cutoff), while the Cartesian formulation employed in the standard model (see equation (2) of Parker *et al.* 1983) is restricted by a representation of the channel centreline as a single-value function. We point out the integro-differential character of the latter equation which is due to its ability to account for the history of the deformation process. Nonlinearity is the second important feature of (2.5); it arises from purely geometrical constraints. Flow nonlinearity may also affect (2.5) provided the dependence of ζ on ϑ is nonlinear. The latter behaviour arises under near resonant conditions. Finally, we note that (2.5) governs the evolution of ϑ, hence of curvature, and in this respect it appears to be the most appropriate form of the evolution equation to check the significance of the field observations of Langbein & Leopold (1964) and Kinoshita (1961).

In order to establish the coupling between the planimetric evolution equation (2.5) and the solution for the flow-bed topography fields we must stipulate a suitable 'erosion law'. The process of meander migration is based on the occurrence of erosion at concave banks and deposition at the convex banks. This is an intermittent process, the details of which are fairly complex. Erosion may be associated with several causes, like bank collapse due to scour at the bank toe or development of tension cracks, groundwater seepage and vegetation (see Mosselman (1989) for a discussion of the various possible mechanisms). However, it proves sufficiently adequate to assume that on the very slow timescale associated with the planimetric development of the channel, the process may be modelled as continuous and that a simple linear law relates ζ to some measure of flow perturbations relative to the uniform configuration assumed to be in equilibrium. In other words, the transient process whereby sediment eroded at concave banks is deposited at convex banks, keeping the channel width constant, is taken to occur instantaneously. Ikeda *et al.* (1981) have assumed that the appropriate measure of flow perturbations determining the transverse rate of migration of the channel is the perturbation of longitudinal velocity u evaluated at the bank. Such an assumption has found some support in the attempt at a mechanistic description of bank erosion by Hasegawa (1989). One may argue in favour of slightly different assumptions such as choosing the perturbation of bottom stress at the bank as an alternative quantity controlling the distribution of ζ. Indeed, as argued by Osman & Thorne (1988), the transverse migration rate of a channel is ultimately controlled by the ability of the stream to remove the sediment accumulating at the bank toe.

However, we have tested the sensitivity of the solution to the choice of different assumptions and found that its qualitative behaviour is not affected. Hence, we follow

Ikeda *et al.* (1981) and stipulate that

$$\zeta = E\left[u|_{n=1} - u|_{n=-1}\right], \tag{2.6}$$

where E is the erodibility coefficient and n the dimensionless transverse coordinate, scaled by B^*.

Note that (2.6) rules out any possible effect on the erosion rate of a symmetric component of u as the latter would lead to widening of the channel, but no shifting of the channel axis.

In order to make any progress, we must employ the solution for the flow-bed topography field of the meandering channel derived in the Part 1.

3. An exact periodic solution for meander development from incipient formation to cutoff

Let us consider a wide curved channel with constant width $2B^*$ and gently sloping banks. Let the channel axis be described by a distribution $\vartheta(s,t)$ such that the dimensionless channel curvature $(-\vartheta_{,s})$ be everywhere small. Hence, we write

$$-\vartheta_{,s} = v_0 \mathscr{C}(s,t), \tag{3.1}$$

with

$$v_0 \equiv \frac{B^*}{R_0^*} \ll 1, \tag{3.2}$$

where R_0^* is some characteristic value of the radius of curvature. In (3.1) $\mathscr{C}(s,t)$ is some $O(1)$ function describing the instantaneous distribution of curvature. We will assume that $\mathscr{C}(s,t)$ can be expanded in Fourier series in the reach considered, such that

$$\mathscr{C}(s,t) = \sum_{m=1}^{\infty} (\mathscr{C}_m e_m + \text{c.c.}), \quad e_m = \exp \mathrm{i}\lambda_m s, \tag{3.3a,b}$$

where both amplitudes $(\mathscr{C}_m)$ and wavenumbers (λ_m) vary on the slow timescale associated with the planimetric development of the channel axis.

Using (2.6) and the expansion (5.11, 5.13) from Part 1 the planimetric evolution equation (2.5) becomes

$$\vartheta_{,t} - e\vartheta_{,s} \sum_{m=0}^{\infty} (-1)^m \int_0^s u_m \vartheta_{,s} \mathrm{d}s = e \sum_{m=0}^{\infty} (-1)^m u_{m,s}, \tag{3.4}$$

where $e = 2Ev_0$ is the modified erosion coefficient.

The solution of the latter equation is then coupled with the solution of the flow problem (5.15)–(5.17) from Part 1.

3.1. *Sine-generated curve and linear bend instability*

The simplest periodic solution of (3.4–5.15 Part 1) under the assumption of linearity is the sine-generated curve of Langbein & Leopold (1964), which then appears to be a theoretically founded result rather than a pure empirical correlation. Indeed assuming

$$\vartheta = \vartheta_1(t) \exp(\mathrm{i}\lambda s) + \text{c.c.}, \tag{3.5}$$

with ϑ_1 taken to be infinitesimal (3.4–5.15 Part 1) reduce to

$$\frac{\mathrm{d}\vartheta_1}{\mathrm{d}t} = G\vartheta_1, \tag{3.6}$$

where

$$G = \frac{e}{v_0}\sum_{m=0}^{\infty}(-1)^m \mathrm{i}\lambda A_m \frac{\sum_{j=1}^{7}\varrho_j(\mathrm{i}\lambda)^j}{\sum_{j=0}^{4}\sigma_j(\mathrm{i}\lambda)^j}. \tag{3.7}$$

This solution represents a regular sequence of small-amplitude meanders of wavenumber λ. They decay or grow depending on whether or not the value of λ exceeds some critical value depending on the parameters β, τ_* and d_s. The latter findings coincide with the predictions of Blondeaux & Seminara (1985). In that paper, it was also shown that for suitable values of λ and β, depending on θ and d_s, the growth rate tends to infinity, which implies the occurrence of resonance. Such a phenomenon was explained in terms of a forcing of a natural response of flow and bed topography consisting of stationary free bars. Furthermore, under sub-resonant conditions, meanders are found to migrate downstream whereas super-resonant conditions imply upstream migration. The change of sign of the migration speed from positive to negative is associated with a progressive shift of the location of maximum flow velocity at the outer bank from downstream to upstream of the bend apex. An experimental verification of the occurrence of such a shift as β crosses the resonant barrier was obtained by Colombini, Tubino & Whiting (1992).

The linear flow solution derived in this section fails under near resonant conditions and a nonlinear solution of the type proposed by Seminara & Tubino (1992) is called for. We exclude from our analysis the occurrence of resonance, i.e. we analyse the process occurring when growth is associated with non-resonant conditions.

3.2. *Kinoshita curve and nonlinear bend instability*

A general periodic solution of (3.4) and (5.15 Part 1) is

$$\vartheta = \sum_{k=1}^{\infty}\vartheta_k(t)\exp[\mathrm{i}\lambda_k(t)s] + \text{c.c.}, \tag{3.8}$$

where

$$\lambda_k = \frac{2\pi}{L(t)}(2k-1) = (2k-1)\lambda(t), \tag{3.9}$$

and $L(t)$ is the intrinsic wavelength of meanders scaled by B^*. The reader will note the peculiarity of the above expansion, which is not a simple Fourier expansion; in fact, in (3.8), the wavenumber of each Fourier mode is time dependent.

At each time, the first two terms of (3.8) identify a Kinoshita-type curve. It will appear from the results presented in the next section that, in the sub-resonant case, spatial harmonics higher than the third do not play any role as cutoff is found to occur before they have had the chance to amplify. Hence, Kinoshita's (1961) observations find theoretical support in the present solution.

Also, note that (3.8) does not contain even harmonics: this is a result of the cubic geometric nonlinearity of the planimetric evolution equation.

Setting

$$(u_m, \zeta) = \sum_{k=1}^{\infty}[(u_{mk}, \zeta_k)\vartheta_k \exp(\mathrm{i}\lambda_k s + \text{c.c.})] \tag{3.10}$$

we find from (2.6) that

$$\zeta_k = \frac{e}{v_0}\sum_{m=0}^{\infty}(-1)^m u_{mk}, \tag{3.11}$$

where, recalling (5.15 Part 1), the coefficients u_{mk} read:

$$u_{mk} = A_m \frac{\sum_{j=1}^{7} \varrho_j (i\lambda_k)^j}{\sum_{j=0}^{4} \sigma_j (i\lambda_k)^j}. \tag{3.12}$$

Substituting from (3.8)–(3.10) into (3.4), equating coefficients of $\exp(\mathrm{i}\lambda_k s)(k = 0, 1, \ldots)$ and imposing that terms linear in s (i.e. non-periodic contributions associated with the integro-differential nonlinearity of (2.5)) should vanish, results in a system of nonlinear ordinary differential equations with cubic nonlinearities for the complex coefficients of the expansion (3.8). If harmonics higher than the fifth are neglected, the resulting system is found to read:

$$\begin{aligned}
\frac{\mathrm{d}\vartheta_1}{\mathrm{d}t} = \mathrm{i}\lambda \{ & \zeta_1\vartheta_1 - \tfrac{1}{2}\zeta_1\vartheta_1^3 - \tfrac{1}{2}(\zeta_1\vartheta_1^2\bar{\vartheta}_1 + \text{c.c.}) - \tfrac{1}{4}(3\zeta_1 + \zeta_3)\vartheta_1^2\vartheta_3 + \tfrac{1}{2}(\bar{\zeta}_3 - 3\zeta_1)\vartheta_1^2\bar{\vartheta}_3 \\
& + \tfrac{1}{2}\zeta_3\bar{\vartheta}_1^2\vartheta_3 + \tfrac{1}{2}(\zeta_3 - 3\bar{\zeta}_1)\vartheta_1\bar{\vartheta}_1\vartheta_3 - \tfrac{1}{4}(3\bar{\zeta}_1 + \bar{\zeta}_3)\vartheta_1\bar{\vartheta}_1\bar{\vartheta}_3 - \tfrac{1}{2}\vartheta_1\left(\zeta_3\vartheta_3^2 + \text{c.c.}\right) \\
& + \tfrac{3}{4}(3\zeta_1 - 2\bar{\zeta}_3 - \zeta_3)\vartheta_1\vartheta_3\bar{\vartheta}_3 + \tfrac{1}{4}(\zeta_5 - 5\zeta_1)\,\vartheta_1\bar{\vartheta}_1\vartheta_5 + \tfrac{1}{4}\left(9\zeta_5 - 5\bar{\zeta}_3\right)\bar{\vartheta}_1\bar{\vartheta}_3\vartheta_5 \\
& + \tfrac{5}{4}\left(\tfrac{5}{3}\zeta_1 - \bar{\zeta}_5 - \tfrac{2}{3}\zeta_5\right)\vartheta_1\vartheta_5\bar{\vartheta}_5 + \tfrac{1}{2}\zeta_5\vartheta_1\vartheta_5^2 - \tfrac{1}{6}(5\zeta_1 + \zeta_5) + \tfrac{1}{4}\left(\bar{\zeta}_5 - 5\zeta_1\right)\vartheta_1^2\bar{\vartheta}_5 \\
& - \tfrac{1}{6}\left(5\bar{\zeta}_1 + \bar{\zeta}_5\right)\vartheta_1\bar{\vartheta}_1\bar{\vartheta}_5 - \tfrac{1}{2}\bar{\zeta}_5\vartheta_1\bar{\vartheta}_5^2 - \tfrac{5}{2}\bar{\zeta}_3\vartheta_1\bar{\vartheta}_3\vartheta_5 - \tfrac{1}{8}\vartheta_1\left[(3\zeta_5 + 5\zeta_3)\,\vartheta_3\vartheta_5 + \text{c.c.}\right] \\
& + \tfrac{1}{2}\left(3\bar{\zeta}_5 - 5\zeta_3\right)\vartheta_1\vartheta_3\bar{\vartheta}_5 + \left(\zeta_3 - \tfrac{9}{2}\bar{\zeta}_5\right)\vartheta_3^2\bar{\vartheta}_5\}\,,
\end{aligned} \tag{3.13}$$

$$\begin{aligned}
\frac{\mathrm{d}\vartheta_3}{\mathrm{d}t} = \mathrm{i}\lambda \{ & 3\zeta_3\vartheta_3 + \tfrac{1}{2}\zeta_1\vartheta_1^3 - \tfrac{3}{2}\zeta_1\vartheta_1^2\vartheta_3 - \tfrac{3}{2}\bar{\zeta}_1\bar{\vartheta}_1^2\vartheta_3 + \tfrac{3}{4}(2\bar{\zeta}_1 - \zeta_1 - \zeta_3)\vartheta_1\bar{\vartheta}_1\bar{\vartheta}_3 \\
& - \tfrac{3}{4}(3\zeta_1 + \zeta_3)\vartheta_1\vartheta_3^2 + \tfrac{3}{2}(\zeta_3 - 3\bar{\zeta}_1)\bar{\vartheta}_1\vartheta_3^2 + \tfrac{3}{2}(\bar{\zeta}_3 - 3\zeta_1)\vartheta_1\vartheta_3\bar{\vartheta}_3 - \tfrac{3}{2}\zeta_5\vartheta_3\zeta_5^2 \\
& - \tfrac{3}{4}(3\bar{\zeta}_1 + \bar{\zeta}_3)\bar{\vartheta}_1\vartheta_3\bar{\vartheta}_3 - \tfrac{3}{2}\zeta_3\vartheta_3^3 - \tfrac{3}{2}(\zeta_3\vartheta_3^2\bar{\vartheta}_3 + \text{c.c.}) + \tfrac{3}{2}\left(3\bar{\zeta}_5 - 5\zeta_3\right) \\
& + \tfrac{15}{2}\left(5\zeta_3 - \bar{\zeta}_5 - \tfrac{\zeta_5}{4}\right)\vartheta_3\vartheta_5\bar{\vartheta}_5 + \tfrac{3}{2}\left(3\zeta_5 - 5\bar{\zeta}_3\right)\vartheta_3\bar{\vartheta}_3\vartheta_5 - \tfrac{3}{2}\bar{\zeta}_5\vartheta_3\bar{\vartheta}_5^2 \\
& - \tfrac{3}{4}\left[\left(\zeta_5 - 5\bar{\zeta}_1\right)\bar{\vartheta}_1\vartheta_3\vartheta_5 + \text{c.c.}\right] + (5\zeta_1 - 2\zeta_5)\,\vartheta_1\bar{\vartheta}_3\vartheta_5 - \tfrac{1}{2}\left(\bar{\zeta}_5 + 5\bar{\zeta}_1\right)\bar{\vartheta}_1\vartheta_3\bar{\vartheta}_5 \\
& + \tfrac{1}{2}(5\zeta_1 + \zeta_5)\,\vartheta_1\vartheta_3\vartheta_5 - \tfrac{3}{8}\left[\left(3\bar{\zeta}_5 + 5\bar{\zeta}_3\right)\bar{\vartheta}_3\bar{\vartheta}_5 + \text{c.c.}\right]\vartheta_3\}\,,
\end{aligned} \tag{3.14}$$

$$\begin{aligned}
\frac{\mathrm{d}\vartheta_5}{\mathrm{d}t} = 5\mathrm{i}\lambda \{ & \zeta_5\vartheta_5\tfrac{1}{2}\zeta_5\vartheta_5^3 + \tfrac{1}{2}\left(\vartheta_5^2\bar{\vartheta}_5\zeta_5 + \text{c.c.}\right) - \tfrac{1}{8}(5\zeta_3 + 3\zeta_5)\,\vartheta_5^2\vartheta_3 \\
& - \tfrac{1}{6}(\zeta_5 + 5\zeta_1)\,\vartheta_1\vartheta_5^2 + \tfrac{1}{4}(\zeta_5 - 5\zeta_1)\,\bar{\vartheta}_1\vartheta_5^2 + \tfrac{1}{2}\left(3\zeta_5 - 5\bar{\zeta}_3\right)\bar{\vartheta}_3\vartheta_5^2 \\
& + \tfrac{1}{20}\,(\zeta_3 + 9\zeta_1)\,\vartheta_1^2\vartheta_3 + \tfrac{1}{5}\left(\tfrac{9}{2}\bar{\zeta}_1 - 2\zeta_3\right)\bar{\vartheta}_1\vartheta_3^2 - \tfrac{1}{2}\vartheta_5\left(\zeta_3\vartheta_3^2 + \zeta_1\vartheta_1^2 + \text{c.c.}\right) \\
& - \tfrac{1}{4}\left(\bar{\zeta}_5 - 5\zeta_1\right)\vartheta_1\vartheta_5\bar{\vartheta}_5 - \tfrac{1}{6}\left(\bar{\zeta}_5 - 5\bar{\zeta}_1\right)\bar{\vartheta}_1\vartheta_5\bar{\vartheta}_5 - \tfrac{1}{8}\left(5\bar{\zeta}_3 + 3\bar{\zeta}_5\right)\bar{\vartheta}_3\vartheta_5\bar{\vartheta}_5 \\
& + \tfrac{1}{2}\left(3\bar{\zeta}_5 - 5\bar{\zeta}_3\right)\vartheta_3\vartheta_5\bar{\vartheta}_5 - \tfrac{3}{8}\left(\zeta_3 + 3\zeta_5 - 4\bar{\zeta}_3\right)\vartheta_3\bar{\vartheta}_3\vartheta_5 - \tfrac{1}{4}[(3\zeta_1 + \zeta_3)\,\vartheta_1\vartheta_3 + \text{c.c.}]\,\vartheta_5 \\
& - \tfrac{1}{12}\left(\zeta_5 + 2\zeta_1 - 3\bar{\zeta}_1\right)\vartheta_1\bar{\vartheta}_1\vartheta_5 + \tfrac{1}{2}\left[\left(\zeta_3 - 3\bar{\zeta}_1\right)\bar{\vartheta}_1\vartheta_3 + \text{c.c.}\right]\vartheta_5\}\,,
\end{aligned} \tag{3.15}$$

$$\frac{\mathrm{d}\lambda}{\mathrm{d}t} = \lambda^2[\mathrm{i}(5\bar{\zeta}_5\vartheta_5\bar{\vartheta}_5 + 3\bar{\zeta}_3\vartheta_3\bar{\vartheta}_3 + \bar{\zeta}_1\vartheta_1\bar{\vartheta}_1) + \text{c.c.}], \tag{3.16}$$

where an overbar denotes the complex conjugate of a complex number.

The nonlinear ordinary differential system (3.13)–(3.16) provides the set of coupled amplitude equations able to describe the nonlinear planimetric development of periodic trains of river meanders starting from an initial sine-generated shape of wavenumber $\lambda(t)|_{t=0}$.

It is instructive to examine a particular case of the latter system, obtained by assuming that all the higher harmonics are negligible with respect to the first. The numerical solution discussed in § 4 will show that, under sub-resonant conditions, even at the late stage of meander development, third harmonics do typically remain much smaller than the fundamental. Under these conditions, the above system reduces to the following form:

$$\frac{\mathrm{d}\vartheta_1}{\mathrm{d}t} = \mathrm{i}\lambda\left[\zeta_1\vartheta_1 - \tfrac{1}{2}\zeta_1\vartheta_1^3 - \tfrac{1}{2}(\zeta_1\vartheta_1^2\bar{\vartheta}_1 + \text{c.c.})\right], \tag{3.17}$$

$$\frac{\mathrm{d}\lambda}{\mathrm{d}t} = \lambda^2[\mathrm{i}\bar{\zeta}_1\vartheta_1\bar{\vartheta}_1 + \text{c.c.}]. \tag{3.18}$$

Note that (3.17) bears some similarity with the classical Landau equation governing the weakly nonlinear evolution of the unstable Fourier mode excited by the hydrodynamic instability of steady basic states. However, the amplitude equation (3.17) differs from the Landau equation owing to the presence of the second and fourth terms in the right-hand side. Furthermore, the coefficients of the linear and cubic terms of (3.17) depend on time through their dependence on the fundamental wavenumber λ and on the coefficient $\zeta_1(\lambda)$. This feature arises from the integrodifferential nature of the original planimetric evolution equation (2.5), which reflects itself in the need to evaluate the instantaneous wavenumber by solving equation (3.18) coupled to equation (3.17). Hence, the history of channel deformation is accounted for through the time development of the fundamental wavenumber λ.

At this stage, it is instructive to attempt answering an important general question: do equilibrium patterns of river meanders exist? In other words, can meanders of permanent form migrate in the longitudinal direction without displaying any growth or decay?

This question was posed and answered by Parker *et al.* (1983, 1986). Parker *et al.* (1983) showed that a nonlinear solution of permanent form does indeed exist in a neighbourhood of the wavenumber characterized by vanishing growth rate. However, such a solution was shown to be unstable by Parker & Andrews (1986). Hence, the conclusion reached confirms the experimental observations which suggest that, in the absence of geological constraints, meanders evolve continuously.

We may readily revisit the above problem using the Landau-type amplitude equation (3.17). In fact, adding (3.17) multiplied by $\bar{\vartheta}_1$ from the complex conjugate of (3.17) multiplied by ϑ_1, we find:

$$2\frac{\mathrm{d}}{\mathrm{d}t}|\vartheta_1|^2 = \mathrm{i}\lambda(\zeta_1 - \bar{\zeta}_1)|\vartheta_1|^2[2 - |\vartheta_1|^2], \tag{3.19}$$

where $|\vartheta_1|$ is the modulus of the complex number ϑ_1. Hence, in order to achieve equilibrium, the meander amplitude, expressed in terms of the real quantity $|\vartheta_1|$, must reach the value $\sqrt{2}$. Figure 4 shows that such conditions can never be reached by a train of sine-generated meander bends, as they correspond to a stage such that cutoffs would have already occurred. Note that such a result is independent of meander wavenumber; however, it relies on the assumption that the dominant contribution to meander shape arises from the fundamental in our expansion (3.8). Hence, the latter result is strongly suggestive of the absence of any equilibrium configuration,

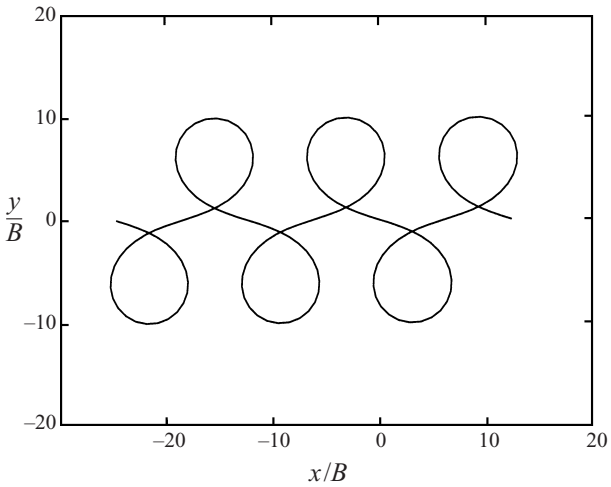

FIGURE 4. First approximation theoretical equilibrium solution of (2.5): $\vartheta_1 = \sqrt{2}$.

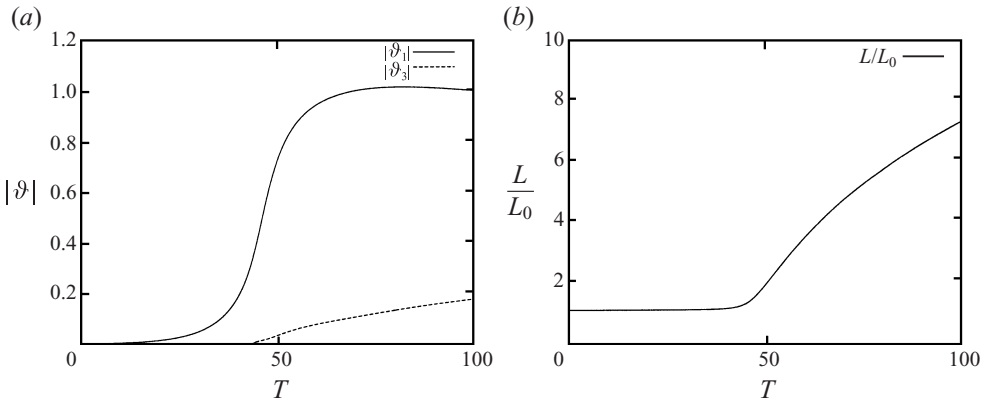

FIGURE 5. Time evolution of (*a*) the amplitude of the first and third harmonic, and (*b*) of normalized intrinsic wavelength for meander evolution reported in figure 6(*a*).

but does not conclusively rule out the possibility that equilibrium might be achieved through the development of more complex shapes with higher harmonics playing a non-negligible role. The numerical experiments discussed below have not shown any such tendency.

4. Planimetric development of river meanders in the sub-resonant and super-resonant cases

We have solved the nonlinear ordinary differential system (3.13)–(3.16) by means of a Runge–Kutta scheme of the fourth order. We have first investigated the sub-resonant case. In order to achieve good accuracy of the integrations, a timestep $\mathrm{d}T = 0.01$ ($T = et$) has been employed. Results are described in figures 5–7.

Figure 5 shows the results of a numerical integration starting from the initial condition $\mathrm{Re}(\vartheta_1) = 0.001$, $\mathrm{Re}(\vartheta_3) = \mathrm{Re}(\vartheta_5) = \mathrm{Im}(\vartheta_1) = \mathrm{Im}(\vartheta_3) = \mathrm{Im}(\vartheta_5) = 0$ with

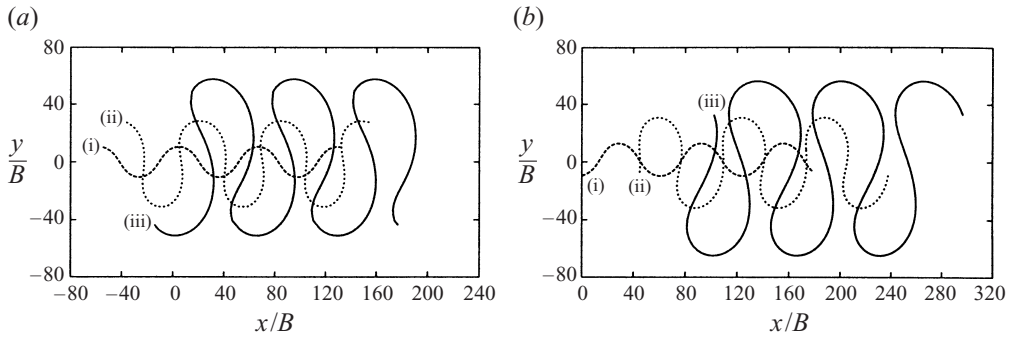

FIGURE 6. (*a*) Sub-resonant evolution of periodic meanders. (*b*) Standard model prediction ($\tau_* = 0.2$, $\beta = 10$, $d_s = 0.01$).

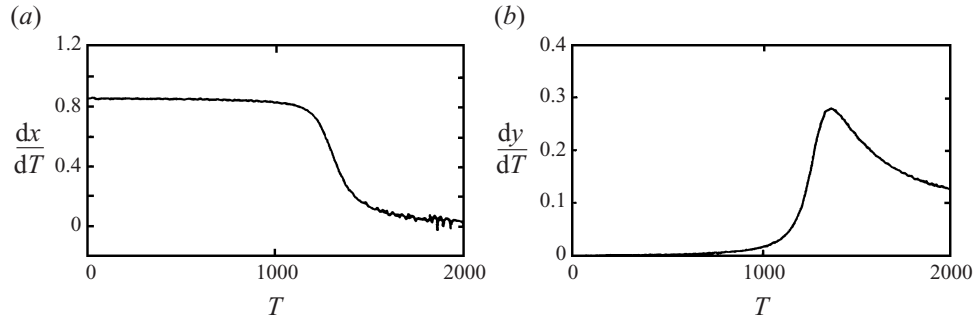

FIGURE 7. (*a*) Lateral migration rate and (*b*) bend amplification as functions of dimensionless time T of meander evolution reported in figure 6(*a*).

the following initial values of the relevant parameters: $\lambda = 0.1$, $\beta = 10$, $\tau_* = 0.2$, $d_s = 0.01$.

It appears that meander development is characterized by two distinct phases: a linear growth of the fundamental, followed by a slower nonlinear growth in which the third harmonic is also excited reaching values of the order of 20 of the fundamental, while the fifth harmonic remains negligible. Figure 5(*b*) shows that, during the linear phase, the meander length increases quite slowly while the process becomes faster in the nonlinear stage.

Figure 6(*a*) shows the development of the planimetric form, from the initial stage to cutoff. Note the progressive fattening and upstream skewing of the meander shape resulting from the role of the third harmonic. The planimetric development found by the present model is quite close to that found by the standard model which is reported in figure 6(*b*).

Figure 7(*a*) shows the time development of the downstream migration speed $\mathrm{d}x/\mathrm{d}T$ which is found to decrease to very small values at the stage immediately before cutoff. Figure 7(*b*) shows that the rate of bend amplification grows to a peak and then slowly decays. Both these findings are in agreement with field observations (see Nanson & Hickin 1983).

Note that the validity of the present approach, which neglects harmonics higher than the fifth, appears to be supported by the fact that the coefficient of the fifth harmonic remains an order of magnitude smaller than that of the fundamental.

The strongly nonlinear solution obtained and discussed in the present section

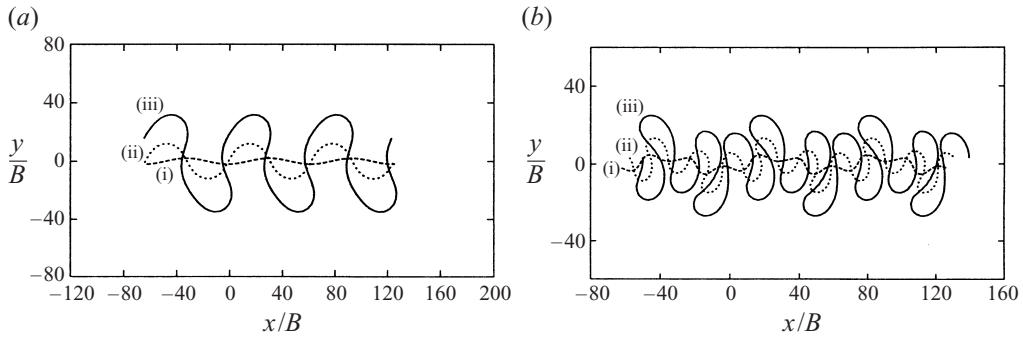

FIGURE 8. (*a*) Super-resonant evolution of periodic meanders. (*b*) Standard model prediction. ($\tau_* = 0.2$, $\beta = 30$, $d_s = 0.01$).

appears to explain the Kinoshita shape developed by large-amplitude meanders and the occurrence of cutoff. Geometric nonlinearities intrinsic in the deformation process appear to be sufficient to give a qualitatively satisfactory insight into the mechanics of the process. The present findings are also in general agreement with the weakly nonlinear analyses of Parker and his coworkers.

A different scenario has been found in the super-resonant case. Figure 8(*a*) shows the planimetric development of meander shape for the same set of parameters employed for the sub-resonant case, except for the width ratio which now exceeds β_R. The distinct features of such a shape are that meanders are skewed downstream and migrate upstream. Such a shape is drastically different from that emerging from the standard model, which is shown in figure 8(*b*).

This difference in skewness may be explained easily in terms of the phase lag δ between the third harmonic and the fundamental; classical upstream skewing occurs when δ lies in the range $(0, \pi)$ whereas δ values in the range $(\pi, 2\pi)$ determine downstream skewing. Figure 9 shows the time behaviour of δ for different values of $\beta_o = \beta|_{t=0}$ before the occurrence of cutoff. The value of δ lies between π and 2π under super-resonant conditions and progressively shifts towards the range $(0, \pi)$ in the sub-resonant regime. Note that cutoff occurs at different times depending on the value of β_0.

In figure 1 we report an example of downstream skewed super-resonant meander, which has been recently observed by W. Dietrich (personal communication). It falls under super-resonant conditions being characterized by the values $\beta = 33.8$ and $\beta_R = 18.2$. The latter value has been obtained using data of the Raggi Island reach of the Fly River reported by Dietrich, Day & Parker (1999), and assuming a value of bankfull discharge ranging about $3000\,\mathrm{m^3\,s^{-1}}$ (W. Dietrich & G. Parker, personal communication).

5. A numerical solution for meander development from initially random patterns

Sequences of fairly regular, periodic meander trains are common in nature, but they usually characterize relatively short reaches of natural rivers. More frequently, meanders exhibit more complex patterns whose irregularity is also due to the occurrence of phenomena such as cutoff processes, spatial heterogeneity of bank erodibility or human constraints which are not accounted for in the present analysis.

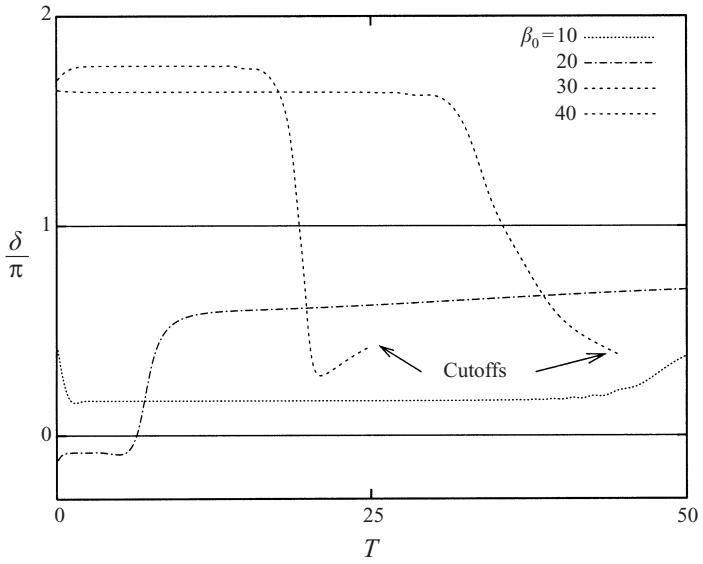

FIGURE 9. Time evolution of the phase lag δ between the third harmonic and the fundamental for different values of the width ratio β_0 ($\tau_* = 0.2$, $d_s = 0.01$).

The effect of the first two features on meander development has been investigated by various authors. Among them, Howard (1992) and Sun *et al.* (1996) performed large time simulations of meander evolution based on the standard model and were able to reproduce intricate meandering patterns.

We show here that irregularity in meandering patterns, i.e. deviations from the classical Kinoshita shape, does not arise only from the three phenomena mentioned above, but is also displayed by the evolution of a meandering reach characterized by an initially random distribution of centreline curvature. Under these conditions, however, the solution of the planimetric evolution equation (2.5) requires numerical integration. Assuming initial conditions consisting of a straight channel axis to which a small-amplitude random perturbation of channel alignment is superimposed, in the super-resonant regime, sequences of irregular meander loops develop before cutoffs occur and under the assumption of spatial homogeneity of the floodplain. The Kinoshita shape characterized either by upstream or downstream skewness and migration rate together with other, commonly observed, meandering patterns (see Brice 1974) like multiple loops may also be reproduced.

A simulation model for meandering rivers was set up following previous numerical schemes already proposed by Howard (1992) and lately improved by Sun *et al.* (1996).

River evolution is described through the planimetric development of the channel centreline, which is discretized as a sequence of points $P_i = (x_i, y_i)$ each of them representing a cross-section of the river identified by a dimensionless streamline coordinate s.

At each timestep Δt, each point of the sequence is shifted orthogonally to the channel centreline by an amount $\zeta \Delta t$, with ζ lateral migration rate discussed in § 2. A new planform of the river is then obtained and the simple numerical procedure is repeated to proceed in the simulation of the planimetric evolution. Note that this approach corresponds to what (2.5) describes analytically; consistency of numerical and analytical solutions was checked in the periodic case and proved to be sharp,

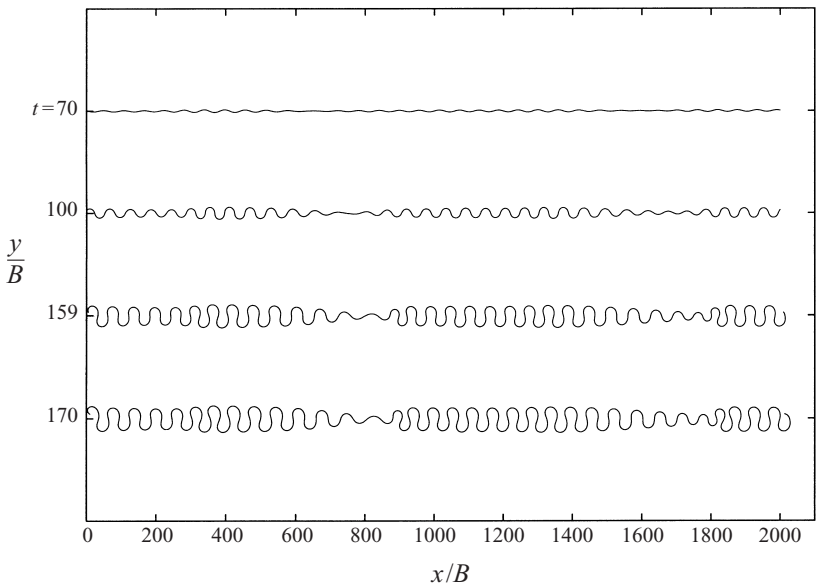

FIGURE 10. Sub-resonant evolution of a randomly perturbed, almost straight, initial channel configuration.

provided the spatial step Δs was smaller than unity. The actual value chosen for Δs was such that the value of the ratio $\Delta s/\Delta t$ was larger than the minimum value for numerical instability to occur.

The local erosion rate ζ is assumed as only parametrically dependent on time on the large timescale of planimetric evolution and is then calculated at each timestep according to the following procedure.

Given the initial planform in the (x, y)-coordinate domain, the distribution $\vartheta(s)$ is obtained by averaging back and forth according to the following expression:

$$\vartheta_i = \frac{1}{2}\left(\arctan\frac{y_{i+1}-y_i}{x_{i+1}-x_i} + \arctan\frac{y_i-y_{i-1}}{x_i-x_{i-1}}\right) \tag{5.1}$$

Curvature and its derivatives are numerically derived through a finite centred difference scheme recalling that $v_0\mathscr{C}(s) = -\mathrm{d}\vartheta/\mathrm{d}s$. The local erosion rate $\zeta(s)$ is then evaluated employing equation (2.6) in which the near-bank perturbation of longitudinal velocity is given by the exact solution (6.1 Part 1). Calculation of ζ for each point of the centreline requires only simple numerical integration to evaluate the convolution integrals discussed in Part 1, § 6. Such integrations were performed by using Simpson's rule.

End conditions were chosen to be periodic, but this choice can be easily replaced with more realistic assumptions; moreover, note that end conditions affect the solution only within a few meander loops of the sequence close to the end sections.

Figures 10 and 11 show the time evolution of the channel centreline under sub- and super-resonant conditions, respectively; the same random initial condition has been employed in the two cases. The maximum initial amplitude of the perturbation is 0.5 B^* and a reach with initial length 2000 B^* is considered. The initial disturbance was obtained by superposition of 100 different harmonics. The initial spectrum is then modified by the evolution process as higher harmonics decay and wavelengths characterized by higher growth rates are naturally selected, as reported in figure 12.

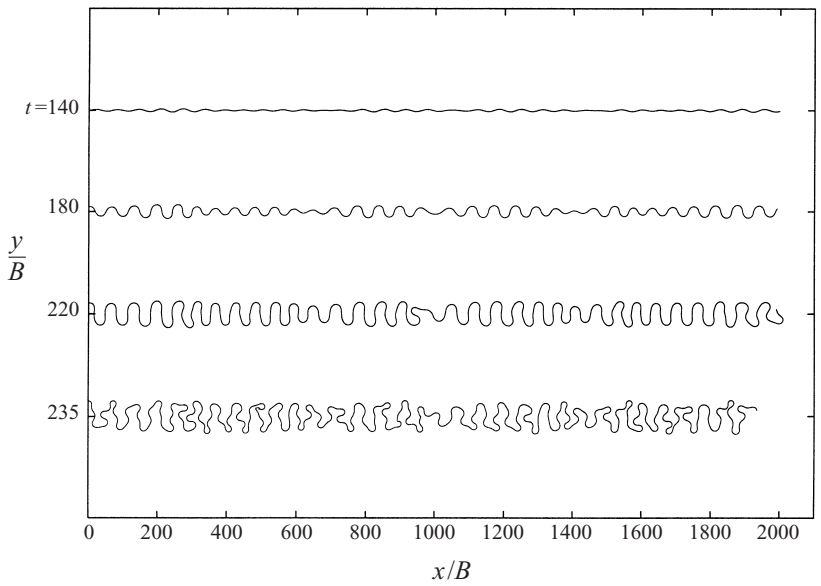

FIGURE 11. Super-resonant evolution of the same initial channel configuration related to figure 10.

Both figures show that selected wavelengths correspond to two or three peaks lying quite close to each other. This suggests that the development of meandering trains is accompanied by the formation of wave groups which are also clearly distinguishable in figure 10. Meander loops almost resembling the classical Kinoshita shape are evidently modulated on a spatial scale corresponding to the wavelength of the envelopes of wave groups. This feature is also clearly noticeable in results presented by Howard (1992) and Sun *et al.* (1996) but it was not pointed out by these authors.

The relevance of the above findings is related to the fact that a similar behaviour is displayed by solutions of the Ginzburg–Landau equation, which describes the nonlinear evolution of unstable perturbations allowing for slow spatial modulations of the most unstable periodic disturbance. Hence, the picture emerging here is quite coherent with the classical picture of nonlinear hydrodynamic instability.

The super-resonant evolution of the same initial pattern considered in the sub-resonant case is reported in figure 11. Simulation is performed by employing the same values of the relevant parameters except for β which now exceeds β_R. It shows the simultaneous development of upstream and downstream skewed meander loops, respectively, characterized by downstream and upstream migration speeds. Such patterns are also sometimes observed in natural streams.

Other commonly observed meandering patterns are reproduced by the present simulations such as multiple loops and other kinds of 'compound loops' described by Brice (1974). In particular, multiple loops are generally due to increasing amplitude of higher harmonics with respect to the amplitude of the fundamental, as shown in the super-resonant spectrum of figure 12.

6. Conclusions

We may now summarize our answers to the questions posed in § 1.

The mechanistic model formulated in Part 1 and in this paper appears to offer a robust and coherent framework able to interpret the main features of meander development from incipient formation to cutoff.

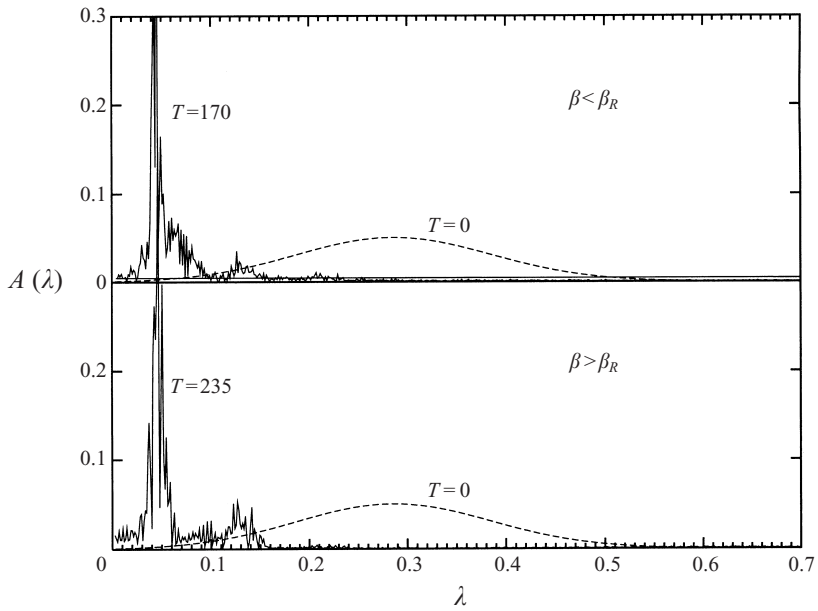

FIGURE 12. The spectrum of the channel axis evolved from characterizing the initial condition of numerical simulations displayed in figures 10 (sub-resonant) and 11 (super-resonant).

In particular, Langbein & Leopold's (1964) sine-generated curve and the Kinoshita curve rather than purely empirical correlations turn out to be the leading and second-order approximations of the exact solution of the planimetric evolution equation, respectively. The absence of even harmonics in such a representation of meander shape is a consequence of the cubic nonlinearity of the planimetric evolution equation.

We have also seen that the main factor controlling the type of meander development is the sub- or super-resonant character of channel flow. In the former regime, which is characterized by a dominant downstream influence, regular trains of meanders migrate downstream and geometric nonlinearities display themselves through an upstream skewing of meander loops which take the classical Kinoshita form. The above scenario is quite similar to that predicted by the standard model. In the super-resonant regime, which is characterized by a dominant upstream morphodynamic influence, the picture reverses and meanders are found to migrate upstream with meander loops skewed downstream. However, note that meander development, increasing the channel length, reduces the basic uniform flow depth keeping roughly the same width of channel. Hence, the width to depth ratio decreases, and the channel regime tends to become sub-resonant in the late stage of meander development.

Also note that no equilibrium solution has been found, though the meander growth rate is found to decrease sharply in the late stage of meander development whereas the migration speed of the meander train is found to decrease monotonically from incipient formation to cutoff. Our findings suggest that equilibrium is not intrinsically impossible, but it cannot be reached as cutoff interrupts the development process.

Further interesting features emerge from our analysis when the initial shape does not consist of a single harmonic, but rather of a spectrum centred on a dominantly unstable harmonic. The response of meander development changes from characteristics typical of Landau-type amplitude equations to those typical of the Ginzburg–Landau evolution equation. In particular, wave groups develop. Furthermore, in the

super-resonant regime, meander shape displays alternating upstream and downstream skewed loops as is sometimes observed in nature. Other typical meandering patterns, such as multiple loops, are also reproduced.

The main question still left open is that of ascertaining to what extent the super-resonant regime overlaps with the regime where braiding occurs. In this respect, note that values of the width to depth ratio required to cross the resonant barrier are fairly large if the bed is plane, but decrease sharply in the dune regime. Hence, while it appears indisputable that the most common scenario is sub-resonant, transient periods of super-resonant development are not unlikely in wide meandering channels (see figure 7 of Part 1).

It has been suggested by one of the referees that super-resonant conditions may also be excited in natural rivers by the commonly observed periodic variations of channel width associated with meander loops. Ascertaining the role of periodic variations of channel width correlated with local bend geometry will indeed deserve some attention in the near future.

Several features of the natural phenomenon have been ignored in the present work. The linearity of the flow model is undoubtedly the first restriction to be removed, though it is quite likely that the picture of meander evolution will not be qualitatively modified by flow nonlinearities. It will be less easy to understand the possible role of migrating features which are present in the initial and late stages of meander growth (Tubino & Seminara 1990; Whiting & Dietrich 1993). Finally, the peculiar case when meander development proceeds from a resonant initial state cannot be covered by the present linear model, it would rather require the use of the weakly nonlinear approach of Seminara & Tubino (1992).

Part of the present results (concerning the periodic sub-resonant case treated analitycally using a simpler flow model) were presented at the '*XXIV Convegno di Idraulica e Costruzioni Idrauliche*' (Seminara, Tubino & Zardi 1994*a*) and at the '*2nd European Fluid Mechanics Conference*' (Seminara *et al.* 1994*b*).

The numerical model discussed in § 5 is entirely due to Guido Zolezzi in partial fulfilment of his PhD thesis.

This work has been jointly supported by the Italian Ministry for Scientific Research (MURST) and by the Universities of Genova and of Trento under the project 'Fluvial and coastal morphodynamics'.

The authors are grateful to W. Dietrich who kindly provided the picture reported in figure 1 and the data on the Fly River.

REFERENCES

Blondeaux, P. & Seminara, G. 1985 A unified bar-bend theory of river meanders. *J. Fluid Mech.* **157**, 449–470.

Brice, J. 1974 Evolution of meander loops. *Geol. Soc. Am. Bull.* **85**, 215–235.

Colombini, M., Tubino, M. & Whiting, P. 1992 Topographic expression of bars in meandering channels. In *Dynamics of Gravel-Bed Rivers* (ed. P. Billi, R. D. Hey, C. R. Thorne & P. Tacconi), pp. 457–474. John Wiley.

Dietrich, W. E., Day, G. & Parker, G. 1999 The Fly River, Papua New Guinea: inferences about river dynamics, floodplain sedimentation and fate of sediment. In *Variety of Fluvial Forms* (ed. A. J. Miller & A. Gupta), pp. 345–376. John Wiley.

Hasegawa, K. 1989 Studies on qualitative and quantitative prediction of meander channel shift. In *River Meandering* (ed. S. Ikeda & G. Parker). AGU Water Resources Monograph 12.

Hickin, E. J. & Nanson, G. C. 1975 The character of channel migration the Beatton River, Northeast British Columbia, Canada. *Geol. Soc. Am. Bull.* **86**, 487–494.

Howard, A. D. 1992 Modelling channel migration and floodplain development in meandering streams. In *Lowland Floodplain Rivers* (ed. P. A. Carling, G. E. Petts). John Wiley.

Ikeda, I., Parker, G. & Sawai, K. 1981 Bend theory of river meanders. Part 1. Linear Development. *J. Fluid Mech.* **112**, 363–377.

Kinoshita, R. 1961 Investigation of channel deformation in Ishikari River. *Rep. Bureau of Resources, Dept Science and Technology, Japan.*

Langbein, W. B. & Leopold, L. B. 1964 Quasi equilibrium states in channel morphology. *Am. J. Sci.* **262**, 782–794.

Mosselman, E. 1989 Theoretical investigation on discharge-induced river bank erosion. *Commun. Hydraul.*, Delft University of Technology, Rep. 3-89.

Nanson, G. C. & Hickin, E. J. 1983 Channel migration and incision on the Beatton River. *J. Hydraul. Div. ASCE* **109**, 327–337.

Osman, A. M. & Thorne, C. R. 1988 Riverbank stability analysis. I: Theory. *J. Hydraul. Engng ASCE* **114**, 134–150.

Parker, G. & Andrews, E. D. 1986 On time development of meander bends. *J. Fluid Mech.* **162**, 139–156.

Parker, G., Diplas, P. & Akiyama, J. 1983 Meander bends of high amplitude. *J. Hydraul. Engng ASCE* **109**, 1323–1337.

Parker, G., Sawai, K. & Ikeda, S. 1982 Bend theory of river meanders, Part 2. Nonlinear deformation of finite-amplitude bends. *J. Fluid Mech.* **115**, 303–314.

Seminara, G. & Tubino, M. 1992 Weakly nonlinear theory of regular meanders. *J. Fluid Mech.* **244**, 257–288.

Seminara, G., Tubino, M. & Zardi, D. 1994*a* Evoluzione planimetrica dei corsi d'acqua meandriformi dall'incipiente formazione al "cut-off". *XXIV Convegno di Idraulica e Costruzioni Idrauliche*, Napoli, 20–22 September, Italy (*in Italian*).

Seminara, G., Tubino, M. & Zardi, D. 1994*b* The development of mature meanders. *2nd European Fluid Mech. Conf.* Warsaw, 20–24 September, Poland.

Speight, J. C. 1965 Meander spectra of the Angabunga River, Papua. *J. Hydrol.* **3**, pp. 1–15.

Speight, J. C. 1967 Spectral analysis of meanders of some Australian rivers. In *Landform Studies from Australia and New Guinea*. Cambridge University Press.

Sun, T., Meaking, P., Jossang, T. & Schwarz, K. 1996 A simulation model for meandering rivers. *Water Resour. Res.* **32**, 2937–2954.

Tubino, M. & Seminara, G. 1990 Free-forced interactions in developing meanders and suppression of free bars. *J. Fluid Mech.* **214**, 131–159.

Whiting, P. J. & Dietrich, W. E. 1993 Experimental studies of bed topography and flow patterns in large-amplitude meanders. 1. Observations. *Water Resour. Res.* **29**, 3605–3622.

Zolezzi, G. & Seminara, G. 2001 Downstream and upstream influence in river meandering. Part 1. General theory and application to overdeepening. *J. Fluid Mech.* **438**, 183–211.